

Proca stars with nonminimal coupling to the Einstein tensor

Masato Minamitsuji^{1,*}

¹*Centro Multidisciplinar de Astrofísica - CENTRA, Instituto Superior Técnico - IST,
Universidade de Lisboa - UL, Avenida Rovisco Pais 1, 1049-001, Portugal.*

(Dated: July 31, 2018)

We investigate Proca star (PS) solutions, namely boson star (BS) type solutions for a complex vector field with mass and nonminimal coupling to the Einstein tensor. Irrespective of the existence of nonminimal coupling, PS solutions are mini-BS type, but the inclusion of it changes properties. For positive nonminimal coupling parameters, PS solutions do not exist for central amplitudes above some certain value due to the singular behavior of the evolution equations. For negative nonminimal coupling parameters, there is no such singular behavior but sufficiently enhanced numerical resolutions are requested for larger amplitudes. Irrespective of the sign of the nonzero nonminimal coupling parameter, PSs with the maximal Arnowitt-Deser-Misner mass and Noether charge are gravitationally bound. Properties of PSs are very similar to those of BSs in scalar-tensor theories including healthy higher-derivative terms.

PACS numbers: 04.40.-b Self-gravitating systems; continuous media and classical fields in curved spacetime, 04.50.Kd Modified theories of gravity.

I. INTRODUCTION

Motivated by the observed acceleration of the Universe, many modified gravity (MG) models have been proposed. These models have been tested in the various contexts of astrophysics and cosmology [1, 2]. It is known that many MG models can be expressed in terms of the subclasses of the Horndeski theories, namely the most general scalar-tensor theories with the second-order equations of motion (EOMs) [3–6]. More recently, the extension of the Horndeski theories to the vector-tensor theories has been explored in Refs. [7–13], which are called the generalized Proca theories, as they also correspond to nonlinear extensions of the massive vector field theory where the $U(1)$ gauge symmetry is explicitly broken.

Properties of compact objects will be very important to distinguish MG models in light of future gravitational wave (GW) observations. The simplest compact objects are black holes (BHs), which in the context of generalized Proca theories have been studied in Refs. [14–19]. These solutions have exhibited nontrivial stealth features for the nontrivial Proca and electric charges. Neutron star (NS) solutions in a subclass of generalized Proca theories with nonminimal coupling to the Einstein tensor were studied in Ref. [17]. In this paper, as a candidate of more exotic compact objects, we investigate boson star (BS) type solutions in the generalized complex Proca theory with mass and nonminimal coupling to the Einstein tensor, namely Proca stars (PSs).¹

BSs are gravitationally bound nontopological solitons constituted by bosonic particles. BS solutions have been firstly constructed for a complex scalar field with mass $\mu^2|\phi|^2$ [20–23]. Mass and radius of BSs are typically $\sim M_p^2/\mu$ and $\sim 1/\mu$, respectively, where $M_p = \sqrt{\hbar c/G} = 1.221 \times 10^{19} \text{ GeV}/c^2$ is the Planck mass.² Thus, for $\mu \sim 1 \text{ GeV}$ close to that of protons and neutrons, the mass of BSs becomes 10^{13} g , which is much smaller than the Chandrasekhar mass for their fermionic counterparts $M_{\text{Ch}} \sim M_p^3/\mu^2 \gtrsim M_{\odot}$, where $M_{\odot} = 1.99 \times 10^{33} \text{ g}$ is the Solar mass. On the other hand, for $\mu \sim 10^{-10} \text{ eV}$, mass and radius of BSs become $\sim M_{\odot}$ and $\sim 10 \text{ km}$, respectively, which may be targets for future GW observations as important as BHs and NSs. See Ref. [24] and references therein for BS solutions for other scalar potentials.

BSs are characterized by several conserved charges. The first is the Arnowitt-Deser-Misner (ADM) mass, which corresponds to the gravitational mass. The second is the Noether charge Q associated with the global internal symmetry in the scalar field sector, where μQ measures the rest mass energy of bosonic particles. Thus, the binding energy of a BS is given by $B := M - \mu Q$. For $B < 0$ a BS is said to be gravitationally bound, while for $B > 0$ the excess energy would be translated into kinetic energy of individual bosons. Radial perturbations of BS solutions have been studied in Refs. [23, 25–27]. Q and M are generically the functions of the amplitude of the scalar field at the center ϕ_0 , i.e., $Q = Q(\phi_0)$ and $M = M(\phi_0)$. It has been shown that the critical solution dividing stable BSs from unstable ones satisfies $dQ/d\phi_0(\phi_{0,c}) = dM/d\phi_0(\phi_{0,c}) = 0$, where $\phi_{0,c}$ describes the critical central amplitude and solutions for $\phi_0 > \phi_{0,c}$ are unstable [27, 28]. Because $B(\phi_{0,c}) = M(\phi_{0,c}) - \mu Q(\phi_{0,c}) < 0$, this critical solution possesses negative binding energy. In other words, $B < 0$ does not necessarily correspond to perturbative stability of BSs. Nevertheless, because stable BS solutions satisfy $B < 0$, we may use it as a necessary condition of stability.

In Ref. [29], BS solutions have been studied for a complex scalar field with nonminimal derivative coupling to the Einstein tensor $G^{\mu\nu}\partial_{\mu}\phi\partial_{\nu}\bar{\phi}$, where $\bar{\phi}$ is the complex conjugate of ϕ , which is analogous to a subclass of the Horndeski theories for a real

* masato.minamitsuji@ist.utl.pt

¹ In this paper, we will distinguish “boson stars (BSs)” and “Proca stars (PSs)” for condensates of complex scalar and vector fields, respectively.

² In the rest, we will work in the units of $c = \hbar = 1$.

scalar field. It has been shown that the inclusion of nonminimal derivative coupling changes properties of BSs. For a massive complex field, for positive nonminimal derivative coupling parameters, the evolution equations to determine the structure of BSs become singular for central amplitudes above some certain value, and as a result no BS solutions exist. On the other hand, for negative nonminimal derivative coupling parameters, the evolution equations do not become singular, but for larger central amplitudes enhanced resolutions are requested. Similar properties have been observed for BSs in the Einstein-Gauss-Bonnet (EGB) [30, 31] and Einstein dilaton Gauss-Bonnet (EdGB) [32] theories.

Recently, BS type solutions for a complex vector field, namely PS solutions, have been studied in Refs. [33–35]. For a massive vector field $\mu^2 A^\mu \bar{A}_\mu$, where \bar{A}_μ is the complex conjugate of A_μ , PSs are mini-BS types with masses $\sim M_p^2/\mu$. The properties of PSs are quite similar to those of BSs, and the critical solution dividing stable and unstable PS solutions corresponds to that with the maximal ADM mass and Noether charge [33]. In this paper, we will investigate PS solutions in the presence of nonminimal coupling to the Einstein tensor $G^{\mu\nu} A_\mu A_\nu$, which is analogous to a subclass of the generalized Proca theories studied in the context of BH physics [14–18]. We will find properties of PSs which are very similar to those of BSs in the complex scalar-tensor theories with healthy higher-derivative interactions.³

The paper is constructed as follows: In Sec. II, we will introduce the generalized complex Proca theory with mass and nonminimal coupling to the Einstein tensor and provide the covariant EOMs. In Sec. III, we will arrange EOMs to a set of the evolution equations in the static and spherically symmetric background to determine the structure of PSs. In Sec. IV, we will numerically construct PS solutions and discuss their properties. Finally, Sec. V will be devoted to giving a brief summary and conclusion.

II. THE GENERALIZED COMPLEX PROCA THEORY WITH MASS AND NONMINIMAL COUPLING TO THE EINSTEIN TENSOR

We consider the generalized complex Proca theory with mass and nonminimal coupling to the Einstein tensor

$$S = \int d^4x \sqrt{-g} \left[\frac{1}{2\kappa^2} R - \frac{1}{4} F^{\mu\nu} \bar{F}_{\mu\nu} - \frac{1}{2} (\mu^2 g^{\mu\nu} - \beta G^{\mu\nu}) A_\mu \bar{A}_\nu \right], \quad (1)$$

where the Greek indices (μ, ν, \dots) run the four-dimensional spacetime, $g_{\mu\nu}$ is the metric tensor, $g^{\mu\nu} := (g_{\mu\nu})^{-1}$ is the inverse metric tensor, $g = \det(g_{\mu\nu})$ is the determinant of $g_{\mu\nu}$, and R and $G_{\mu\nu}$ are the Ricci scalar curvature and the Einstein tensor associated with $g_{\mu\nu}$. A_μ is the complex vector field, $F_{\mu\nu} := \partial_\mu A_\nu - \partial_\nu A_\mu$ is the field strength, quantities with a “bar” are the complex conjugates of those without a “bar”, $\kappa^2 := 8\pi G$, G is the gravitational constant, μ^2 is mass of the complex vector field, and β measures nonminimal coupling to the Einstein tensor. In our units, the Planck mass M_p is given by $M_p = 1/\sqrt{G}$.

We obtain EOMs by varying the action Eq. (1) with respect to $g_{\mu\nu}$ and A_μ , respectively. Varying Eq. (1) with respect to $g_{\mu\nu}$, we obtain the gravitational EOM

$$0 = \mathcal{E}_{\mu\nu} := T_{\mu\nu}^{(f)} + \beta T_{\mu\nu}^{(A)} - \frac{1}{\kappa^2} G_{\mu\nu}, \quad (2)$$

where

$$T_{\mu\nu}^{(f)} := \frac{1}{2} F_{\mu\rho} \bar{F}_{\nu}{}^\rho + \frac{1}{2} \bar{F}_{\mu\rho} F_{\nu}{}^\rho - \frac{1}{4} g_{\mu\nu} F^{\rho\sigma} \bar{F}_{\rho\sigma} + \frac{\mu^2}{2} (A_\mu \bar{A}_\nu + A_\nu \bar{A}_\mu) - \frac{\mu^2}{2} g_{\mu\nu} A^\rho \bar{A}_\rho \quad (3)$$

represents the energy-momentum tensor for the ordinary massive Proca field, and

$$\begin{aligned} T_{\mu\nu}^{(A)} := & \frac{1}{2} \left(A^\rho \bar{A}_\rho G_{\mu\nu} + \frac{1}{2} R A_\mu \bar{A}_\nu + \frac{1}{2} R \bar{A}_\mu A_\nu \right) \\ & - \frac{1}{2} g_{\mu\nu} \left(\nabla^\rho A_\rho \nabla^\sigma \bar{A}_\sigma - 2 \nabla^\rho A^\sigma \nabla_\rho \bar{A}_\sigma + \nabla^\rho A^\sigma \nabla_\sigma \bar{A}_\rho - A_\rho \square \bar{A}^\rho - \bar{A}_\rho \square A^\rho + A^\rho \nabla_\rho \nabla_\sigma \bar{A}^\sigma + \bar{A}^\rho \nabla_\rho \nabla_\sigma A^\sigma \right) \\ & - \left(\frac{1}{2} \nabla_\mu A^\rho \nabla_\nu \bar{A}_\rho + \frac{1}{2} \nabla_\mu \bar{A}^\rho \nabla_\nu A_\rho - \frac{1}{2} \nabla^\rho A_\rho \nabla_{(\mu} \bar{A}_{\nu)} - \frac{1}{2} \nabla^\rho \bar{A}_\rho \nabla_{(\mu} A_{\nu)} \right. \\ & - \frac{1}{2} \nabla_\rho A_{(\mu} \nabla_{\nu)} \bar{A}^\rho - \frac{1}{2} \nabla_\rho \bar{A}_{(\mu} \nabla_{\nu)} A^\rho + \frac{1}{2} \nabla_\rho A_\mu \nabla^\rho \bar{A}_\nu + \frac{1}{2} \nabla_\rho A_\nu \nabla^\rho \bar{A}_\mu \\ & + \frac{1}{2} A_\rho \nabla_{(\mu} \nabla_{\nu)} \bar{A}^\rho + \frac{1}{2} \bar{A}_\rho \nabla_{(\mu} \nabla_{\nu)} A^\rho - \frac{1}{2} A^\rho \nabla_\rho \nabla_{(\mu} \bar{A}_{\nu)} - \frac{1}{2} \bar{A}^\rho \nabla_\rho \nabla_{(\mu} A_{\nu)} \\ & \left. + \frac{1}{2} A_{(\mu} \square \bar{A}_{\nu)} + \frac{1}{2} \bar{A}_{(\mu} \square A_{\nu)} - A_{(\mu} \nabla_{\nu)} \nabla_\sigma \bar{A}^\sigma - \bar{A}_{(\mu} \nabla_{\nu)} \nabla_\sigma A^\sigma + \frac{1}{2} A_{(\mu} \nabla_\rho \nabla_{|\nu)} \bar{A}^\rho + \frac{1}{2} \bar{A}_{(\mu} \nabla_\rho \nabla_{|\nu)} A^\rho \right) \end{aligned} \quad (4)$$

³ By “healthy,” we mean that there are no ghosty degrees of freedom associated with Ostrogradsky’s theorem [36].

represents the effective energy-momentum tensor for nonminimal coupling to the Einstein tensor. Similarly, varying Eq. (1) with respect to A_μ and \bar{A}_μ , we obtain the EOM for the complex vector field

$$0 = \mathcal{F}_\nu := \nabla^\mu F_{\mu\nu} - (\mu^2 \delta_\nu^\mu - \beta G_\nu^\mu) A_\mu, \quad (5)$$

and its complex conjugate $\bar{\mathcal{F}}_\nu = 0$, respectively. The $U(1)$ gauge symmetry is explicitly broken by mass and nonminimal coupling. By taking the derivative of Eq. (5), we obtain

$$0 = \mathcal{G} := \mu^2 \nabla^\mu A_\mu - \beta G^{\mu\nu} \nabla_\mu A_\nu, \quad (6)$$

which generalizes the constraint relation for $\beta = 0$, $\nabla^\mu A_\mu = 0$. In the theory (1), there is still global $U(1)$ symmetry under $A_\mu \rightarrow e^{i\alpha} A_\mu$, where α is a constant. The associated Noether current is given by

$$j^\mu = \frac{i}{2} (\bar{F}^{\mu\nu} A_\nu - F^{\mu\nu} \bar{A}_\nu), \quad (7)$$

which satisfies the conservation law $\nabla_\mu j^\mu = 0$.

III. PROCA STARS

A. Static and spherically-symmetric spacetime

In this section, we discuss PSs in the theory (1). We consider a static and spherically symmetric spacetime

$$g_{\mu\nu} dx^\mu dx^\nu = -\sigma(r)^2 \left(1 - \frac{2m(r)}{r}\right) dt^2 + \left(1 - \frac{2m(r)}{r}\right)^{-1} dr^2 + r^2 d\Omega_2^2, \quad (8)$$

where \hat{t} and r are the time and radial coordinates, $d\Omega_2^2$ is the metric of the unit two sphere, and $m(r)$ and $\sigma(r)$ depend only on the radial coordinate r . Correspondingly, we consider the ansatz for the vector field [33]

$$A_\mu dx^\mu = e^{-i\hat{\omega}\hat{t}} (a_0(r) d\hat{t} + i a_1(r) dr), \quad (9)$$

where $a_0(r)$ and $a_1(r)$ depend only on r . We assume that the frequency $\hat{\omega}$ is real, ensuring that the vector field neither grows nor decays. Equation (9) avoids the restrictions from Derrick's theorem that forbid stable localized solutions to nonlinear wave equations [37]. The explicit time dependence $e^{-i\hat{\omega}\hat{t}}$ does not induce the time dependence in the metric. In order to find $m(r)$, $\sigma(r)$, $a_0(r)$, and $a_1(r)$, we solve the evolution equation derived from EOMs (2), (5), and (6).

From our ansatz (8) and (9), the (\hat{t}, \hat{t}) , (r, r) and angular components of the gravitational EOM (2)

$$\mathcal{E}^{\hat{t}}_{\hat{t}} = 0, \quad \mathcal{E}^r_r = 0, \quad \mathcal{E}^i_i = 0, \quad (10)$$

are given by Eq. (A1) with Eq. (A2). Similarly, the t and r components of the vector field EOM (5),

$$\mathcal{F}_{\hat{t}} = 0, \quad \mathcal{F}_r = 0, \quad (11)$$

are given by Eq. (A3) with Eq. (A4). Finally, Eq. (6) is given by Eq. (A5) with Eq. (A6). These equations are constrained by the identity

$$\nabla_\mu \mathcal{E}^\mu_r = -\frac{1}{2} g^{\hat{t}\hat{t}} (\mathcal{F}_{\hat{t}} \times \bar{F}_{\hat{t}r} + \bar{\mathcal{F}}_{\hat{t}} \times F_{\hat{t}r}) + \frac{1}{2} (\mathcal{G} \bar{A}_r + \bar{\mathcal{G}} A_r). \quad (12)$$

Combining them, we obtain a set of the evolution equations (B1a), (B1b), (B1c), and (B5) which determine the structure of PSs from the center $r = 0$ to spatial infinity $r = \infty$.

B. Center

Solving EOMs near the center $r = 0$, we obtain the boundary conditions

$$a_0(r) = f_0 + \frac{f_0}{6} \left\{ \left(\mu^2 - \frac{\hat{\omega}^2}{\sigma_0^2} \right) + \frac{f_0^2 \kappa^2}{2\sigma_0^2} \left(\mu^2 - \frac{2\hat{\omega}^2}{\sigma_0^2} \right) \beta + \frac{f_0^2 \kappa^2}{36\mu^2 \sigma_0^6} (3f_0^2 \mu^2 \kappa^2 (3\mu^2 \sigma_0^2 - 14\hat{\omega}^2) + 4\hat{\omega}^2 (9\mu^2 \sigma_0^2 - 8\hat{\omega}^2)) \beta^2 + O(\beta^3) \right\} r^2 + O(r^4), \quad (13a)$$

$$a_1(r) = -\frac{f_0 \hat{\omega}}{3\sigma_0^2} \left\{ 1 + \frac{f_0^2 \kappa^2}{\sigma_0^2} \beta + \frac{f_0^2 \kappa^2}{18\mu^2 \sigma_0^4} (21f_0^2 \mu^2 \kappa^2 - 12\mu^2 \sigma_0^2 + 16\hat{\omega}^2) \beta^2 + O(\beta^3) \right\} r + O(r^3), \quad (13b)$$

$$m(r) = \frac{f_0^2 \kappa^2}{12\sigma_0^2} \left\{ \mu^2 + \frac{3f_0^2 \mu^2 \kappa^2 + 4\hat{\omega}^2}{6\sigma_0^2} \beta + \frac{3f_0^4 \mu^2 \kappa^4 + 20f_0^2 \kappa^2 \hat{\omega}^2}{12\sigma_0^4} \beta^2 + O(\beta^3) \right\} r^3 + O(r^5), \quad (13c)$$

$$\sigma(r) = \sigma_0 + \frac{f_0^2 \kappa^2}{\sigma_0} \left\{ \frac{\mu^2}{4} + \frac{3f_0^2 \mu^2 \kappa^2 - 3\mu^2 \sigma_0^2 + 4\hat{\omega}^2}{18\sigma_0^2} \beta + \frac{f_0^2 \kappa^2}{48\sigma_0^4} (5f_0^2 \mu^2 \kappa^2 - 8\mu^2 \sigma_0^2 + 20\hat{\omega}^2) \beta^2 + O(\beta^3) \right\} r^2 + O(r^4). \quad (13d)$$

With Eq. (13), we numerically integrate Eqs. (B1a), (B1b), (B1c), and (B5) toward the spatial infinity $r = \infty$. From Eq. (13), for $f_0 = 0$ we obtain $\sigma(r) = \sigma_0$ and $m(r) = a_0(r) = a_1(r) = 0$, namely the Minkowski solution.

C. Spatial infinity

For a correct eigenvalue of $\hat{\omega}$, we find the asymptotically flat solution where $m(r)$ and $\sigma(r)$ exponentially approach constant values, $m_\infty > 0$ and $\sigma_\infty > 0$, respectively, while $a_0(r)$ and $a_1(r)$ exponentially approach zero as $e^{-\sqrt{\mu^2 - \hat{\omega}^2}/\sigma_\infty^2 r}$. Thus, in the large r limit the metric exponentially approaches the Schwarzschild form

$$ds^2 \rightarrow -\sigma_\infty^2 \left(1 - \frac{2m_\infty}{r} \right) d\hat{t}^2 + \left(1 - \frac{2m_\infty}{r} \right)^{-1} dr^2 + r^2 d\Omega_2^2, \quad (14)$$

where the proper time measured at $r = \infty$ is given by $t = \sigma_\infty \hat{t}$, and correspondingly the proper frequency ω is given by

$$\omega := \frac{\hat{\omega}}{\sigma_\infty}. \quad (15)$$

The exponential fall-off condition $e^{-\sqrt{\mu^2 - \hat{\omega}^2} r}$ requires $\omega < \mu$. We numerically confirmed that in the limit $f_0 \rightarrow 0$, namely in the limit of the Minkowski solution, $\omega \rightarrow \mu$, leaving no r dependence in the large r limit.

D. ADM mass, Noether charge, effective radius, and compactness

Having numerical solutions, we then evaluate the conserved quantities which characterize PSs. The first is associated with the time translational symmetry and corresponds to the ADM mass

$$M := \frac{m_\infty}{G} = M_p^2 m_\infty. \quad (16)$$

The second is the Noether charge associated with the global $U(1)$ symmetry, which is given by integrating $j^{\hat{t}}$ in Eq. (7) over a constant time hypersurface

$$Q = \int_{\Sigma} d^3 x \sqrt{-g} j^{\hat{t}} = 4\pi \int_0^\infty dr \frac{r^2 a_1(r) (\hat{\omega} a_1(r) - a_0'(r))}{\sigma(r)}. \quad (17)$$

As for a BS, a PS is said to be gravitationally bound if

$$B := M - \mu Q < 0. \quad (18)$$

As for BSs mentioned in Sec. I, for PSs we use Eq. (18) as a necessary condition for stability.

We then define the effective radius [24]

$$\mathcal{R} := \frac{1}{Q} \int_{\Sigma} d^3x \sqrt{-g} \left(r j^t \right) = \frac{4\pi}{Q} \int_0^{\infty} dr \frac{r^3 a_1(r) (\hat{\omega} a_1(r) - a'_0(r))}{\sigma(r)}, \quad (19)$$

and the (effective) compactness

$$\mathcal{C} := \frac{GM}{\mathcal{R}} = \frac{M}{M_p^2 \mathcal{R}} = \frac{m_{\infty}}{\mathcal{R}}. \quad (20)$$

In contrast to the cases of BHs and NSs, for PSs $r = \mathcal{R}$ is not the surface of $A_{\mu} = 0$. Nevertheless, due to the exponential falloff property of A_{μ} , \mathcal{R} represents the characteristic length scale of energy localization. The parameter \mathcal{C} is very important to distinguish various compact objects in different theories in light of future GW observations.

E. Parameters

For numerical analyses, we may fix some parameters to unity. First, by rescaling

$$\hat{\omega} \rightarrow \frac{\hat{\omega}}{\mu}, \quad r \rightarrow r\mu, \quad m(r) \rightarrow \mu m(r), \quad \sigma(r) \rightarrow \sigma(r) \quad a_0(r) \rightarrow \kappa a_0(r), \quad a_1(r) \rightarrow \kappa a_1(r), \quad (21)$$

we can rewrite Eqs. (B1a), (B1b), (B1c), and (B5) into equations without μ and κ . Hence, we may work by setting $\mu = \kappa = 1$. Moreover, as σ_0 corresponds to the time rescaling at the center $r = 0$, we may also set $\sigma_0 = 1$ for convenience. In general, then $\sigma_{\infty} \neq 1$ and quantities measured at the spatial infinity can be obtained by performing the rescalings discussed in Sec. III C. Thus, the only remaining parameters are f_0 and β . For a fixed value of β , by varying f_0 we numerically integrate them and evaluate the above quantities. In Fig. 1, by setting $\mu = \kappa = \sigma_0 = 1$, $m(r)$, $\sigma(r)$, $a_0(r)$, and $a_1(r)$ are shown as functions of r for $\beta = 0.2$ and $f_0 = 1.0$, which are very similar to the case of $\beta = 0$ [33, 34].

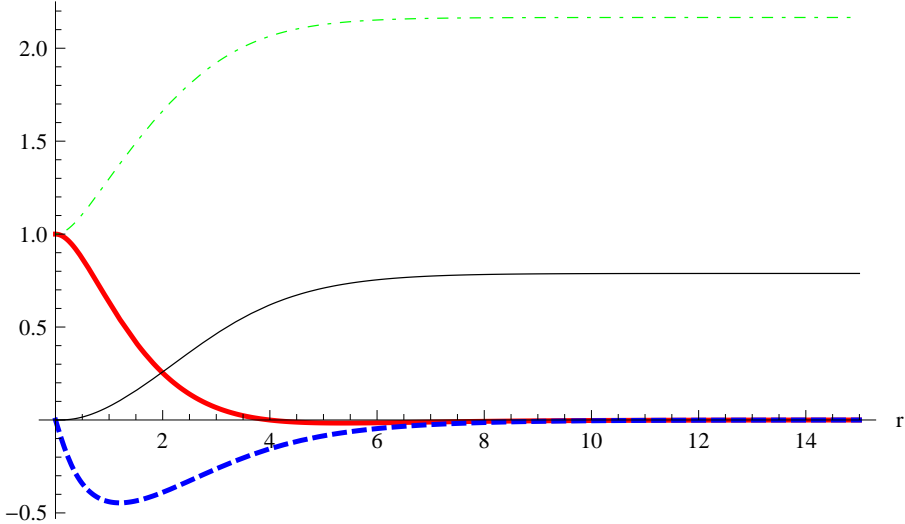


FIG. 1. $m(r)$, $\sigma(r)$, $a_0(r)$, and $a_1(r)$ are shown as functions of r for $\beta = 0.2$ and $f_0 = 1.0$. The solid black, green dotted-dashed, thick red, and thick blue dashed curves correspond to $m(r)$, $\sigma(r)$, $a_0(r)$, and $a_1(r)$, respectively. Here, we set $\mu = \kappa = \sigma_0 = 1$.

Before proceeding, we briefly comment on the massless case $\mu = 0$. In this case, by rescaling

$$r \rightarrow \hat{\omega}r, \quad m \rightarrow \hat{\omega}m, \quad a_0(r) \rightarrow \kappa a_0(r), \quad a_1(r) \rightarrow \kappa a_1(r), \quad (22)$$

the dependence on $\hat{\omega}$ is completely eliminated from EOMs. Thus, the problem does not reduce to the eigenvalue one. As β is dimensionless, for $\mu = 0$ there is no physical scale which characterizes PSs. Thus, there is no PS solution only by nonminimal coupling.

IV. NUMERICAL SOLUTIONS

For each of $\beta = 0.2, 0.1, 0, -0.1$, and -0.2 , for different values of f_0 we numerically integrate the equations (B1a), (B1b), (B1c) and (B5) with the boundary conditions (13), and find ω that reproduces the asymptotic behaviors discussed in Sec. III C. We then evaluate M , Q , \mathcal{R} , and \mathcal{C} discussed in Sec. III D.

A. Frequency

In Fig. 2, for $\beta = 0.2, 0.1, 0, -0.1$, and -0.2 , ω/μ is shown as a function of f_0 . In all cases, for $f_0 \rightarrow 0$, $\omega/\mu \rightarrow 1$ which reproduces the Minkowski solution.

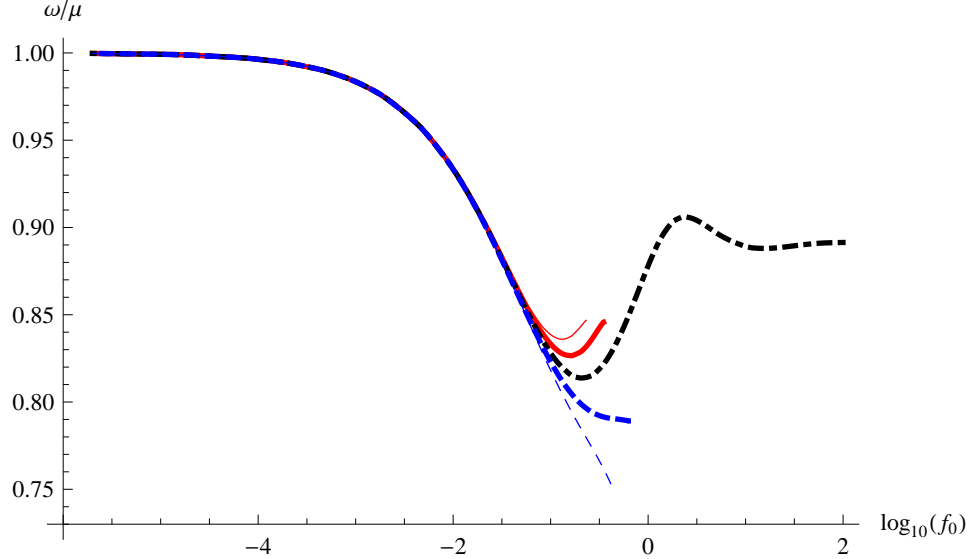


FIG. 2. ω/μ is shown as the function of f_0 . The solid red, thick red, thick black dotted-dashed, thick blue dashed, and blue dashed curves correspond to $\beta = 0.2, 0.1, 0, -0.1$, and -0.2 respectively. f_0 is shown in M_p .

For $\beta = 0$, there are several branches of PSs for a single value of ω . As f_0 increases from zero, ω/μ decreases from 1 and reaches the minimal value 0.814 for $f_0 \approx 0.199M_p$. Then, ω/μ increases and reaches the local maximal value 0.906 for $f_0 \approx 2.39M_p$. As f_0 increases further, ω/μ gradually approaches 0.891. For nonzero values of β , irrespective of its sign, numerical PS solutions cease to exist for f_0 above some certain value. However, the reasons are different for $\beta > 0$ and $\beta < 0$.

For $\beta > 0$, there are several branches of PSs for a single value of ω . However, for f_0 above some certain value depending on β , $\tilde{\mathcal{C}}_1$ in Eq. (B5) always vanishes at a very small radius, and no PS solutions exist. In our examples, no PS solutions are found for $f_0 \gtrsim 0.349M_p$ for $\beta = 0.1$ and for $f_0 \gtrsim 0.231M_p$ for $\beta = 0.2$. Before reaching these values of f_0 , ω/μ takes the minimal values 0.827 for $f_0 \approx 0.160M_p$ ($\beta = 0.1$) and 0.836 for $f_0 \approx 0.140M_p$ ($\beta = 0.2$). Thus, for larger nonminimal coupling parameters, PS solutions cease to exist for smaller amplitudes.

For $\beta < 0$, ω/μ always decreases. Although $\tilde{\mathcal{C}}_1$ in Eq. (B5) does not vanish at any radius, it becomes extremely small for larger values of f_0 , making numerical integrations unstable unless sufficiently high resolutions are taken. Thus, although we will show PS solutions only for smaller values of f_0 where numerical integration can be performed stably, in principle it does not forbid the existence of PS solutions for larger values of f_0 . In our analysis, numerical integration could not be performed stably for $f_0 \lesssim 0.628M_p$ for $\beta = -0.1$ and for $f_0 \lesssim 0.409M_p$ for $\beta = -0.2$.

B. ADM mass and Noether charge

In Figs. 3-5, for $\beta = 0, 0.2$, and -0.2 , M and μQ are shown as functions of ω/μ . For all cases, $f_0 = 0$ gives the Minkowski solution $M = Q = 0$ with $\omega = \mu$. Moreover, even in the presence of the nonminimal coupling to the Einstein tensor PS solutions obtained in our analysis are mini-BS type, where M and μQ are typically $\sim M_p^2/\mu$.

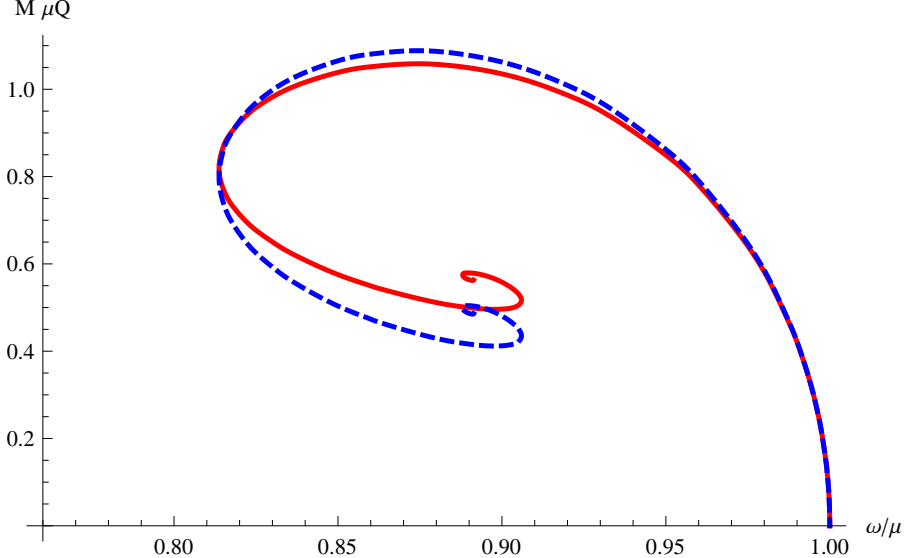


FIG. 3. For $\beta = 0$, M and μQ are shown as functions of ω/μ . The solid red and blue dashed curves correspond to M and μQ , respectively. Here, M and μQ are shown in M_p^2/μ .

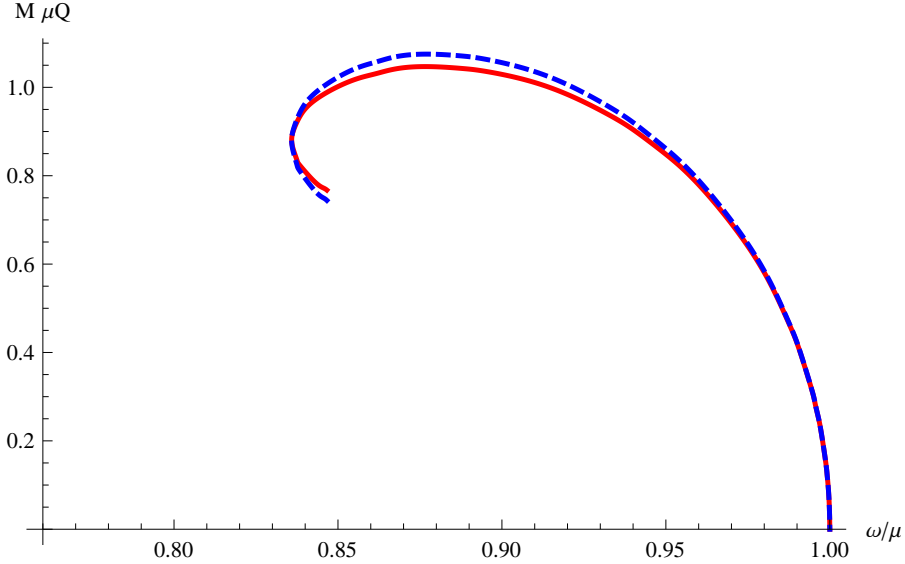


FIG. 4. For $\beta = 0.2$, M and μQ are shown as functions of ω/μ . The solid red and blue dashed curves correspond to M and μQ , respectively. Here, M and μQ are shown in M_p^2/μ .

The case of $\beta = 0$ is shown in Fig. 3. As f_0 increases from zero, M and μQ increase from zero while ω/μ decreases from 1. M and Q then take their maximal values, $M_{\max} \approx 1.06M_p^2/\mu$ and $\mu Q_{\max} \approx 1.09M_p^2/\mu$ for $\omega/\mu \approx 0.870$, which satisfies Eq. (18) and agrees with Ref. [33]. Then ω/μ still decreases, while M and μQ start to decrease. After ω/μ reaches its minimal value 0.814, it starts to increase while M and μQ still decrease until reaching their local minimum values, $M_{\min} \approx 0.496M_p^2/\mu$ and $\mu Q_{\min} \approx 0.412M_p^2/\mu$, respectively. In this region, Eq. (18) is not satisfied. As f_0 increases further, M and μQ eventually converge to $M \approx 0.563M_p^2/\mu$ and $\mu Q \approx 0.486M_p^2/\mu$, respectively.

The case of $\beta = 0.2$ is shown in Fig. 4. As f_0 increases from zero, M and μQ increase from zero while ω/μ decreases from 1. M and μQ then take their maximal values, $M_{\max} \approx 1.05M_p^2/\mu$ and $\mu Q_{\max} \approx 1.07M_p^2/\mu$, for $\omega/\mu \approx 0.872$, which satisfies Eq. (18). Then as ω/μ still decreases, M and μQ start to decrease. After ω/μ reaches its minimal value 0.836, ω/μ starts to increase while M and μQ still decrease. In this region, Eq. (18) is not satisfied. As we discussed in Sec. IV A, for $\beta = 0.2$, we

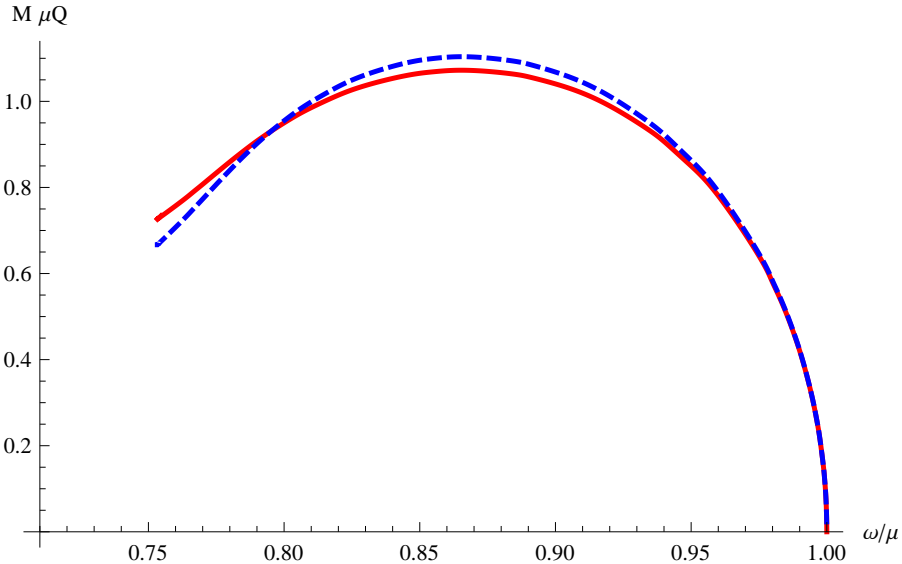


FIG. 5. For $\beta = -0.2$, M and μQ are shown as functions of ω/μ . The solid red and blue dashed curves correspond to M and μQ , respectively. Here, M and μQ are shown in M_p^2/μ .

can obtain PS solutions up to $f_0 = 0.231M_p$, for which $M \approx 0.768M_p^2/\mu$ and $\mu Q \approx 0.744M_p^2/\mu$.

Finally, the case of $\beta = -0.2$ is shown in Fig. 5. As f_0 increases from zero, M and μQ increase from zero while ω/μ decreases from 1. M and μQ then take their maximal values, $M_{\max} \simeq 1.07M_p^2/\mu$ and $\mu Q_{\max} \simeq 1.10M_p^2/\mu$ for $\omega/\mu \approx 0.868$, which satisfies Eq. (18). As f_0 increases further, M and μQ decrease while ω still decreases. As we discussed in Sec. IV A, for $\beta = -0.2$, for f_0 above $0.409M_p$, we could not find numerical PS solutions due to the problem discussed in Sec. IV A. For $f_0 = 0.409M_p$, $M \approx 0.727M_p^2/\mu$ and $\mu Q \approx 0.667M_p^2/\mu$. For $\omega/\mu \lesssim 0.792$, Eq. (18) is not satisfied.

In Fig. 6, M (the left panel) and μQ (the right panel) are shown for all $\beta = 0.2, 0.1, 0, -0.1$, and -0.2 . M and μQ almost coincide for larger ω/μ , i.e., smaller f_0 . As M and μQ approach their maximal values, β dependence becomes more evident, and for negative (positive) values of β , both M and μQ take larger (smaller) values than those for $\beta = 0$ for the same ω . Moreover, for both positive and negative values of β , spiraling features observed for $\beta = 0$ eventually disappear. Such behaviors are very similar to those observed for BSs in the EGB theory [30, 31], the EdGB theory [32] and the complex scalar-tensor theory with nonminimal derivative coupling to the Einstein tensor [29]. Thus, they may be generic for healthy higher-derivative theories.

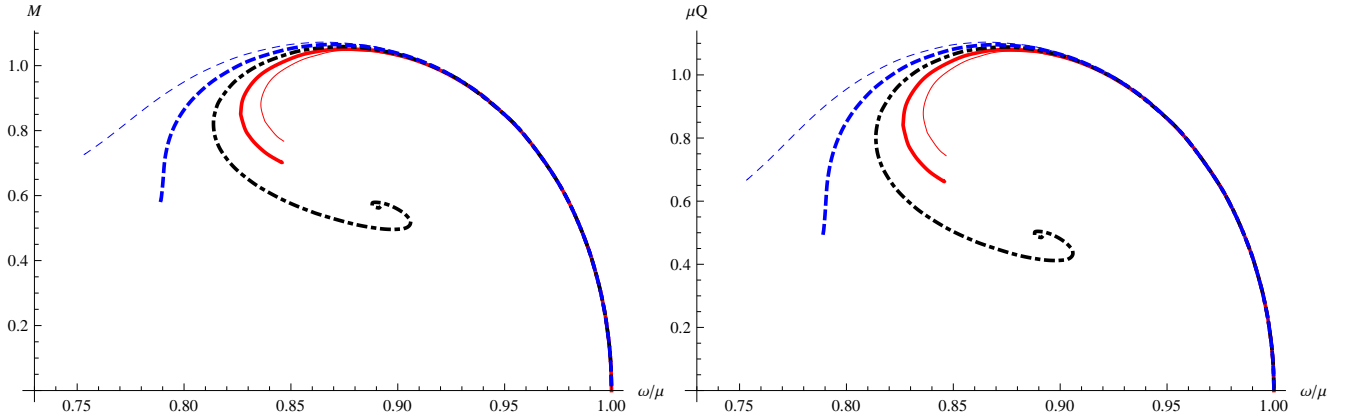


FIG. 6. M (the left panel) and μQ (the right panel) are shown as functions of ω/μ . In each panel, the solid red, thick red, black dotted-dashed, thick blue dashed, and blue dashed curves correspond to $\beta = 0.2, 0.1, 0, -0.1$, and -0.2 , respectively. Here, M and μQ are shown in M_p^2/μ .

C. Mass-radius relation

In Fig. 7, for $\beta = 0.2, 0.1, 0, -0.1$, and -0.2 , M is shown as a function of $\mu\mathcal{R}$ defined in Eq. (19). In all cases, for larger f_0 , \mathcal{R} becomes smaller, which means that energy is localized more efficiently around the center. For $\mu\mathcal{R} \gtrsim 6.0$, no clear β dependence is observed, while for $\mu\mathcal{R} \lesssim 6.0$, β dependence becomes more evident and a larger (smaller) value of M is observed for $\beta < 0$ ($\beta > 0$). For $\beta = 0$, M is a multivalued function of \mathcal{R} , while for $\beta \neq 0$, it is a single-valued function of \mathcal{R} . Very similar behaviors are observed also for μQ as a function of $\mu\mathcal{R}$. As a reference, we also show the case of $\mathcal{R} = 2m_\infty$, although \mathcal{R} has nothing to do with the Schwarzschild radius of a BH.

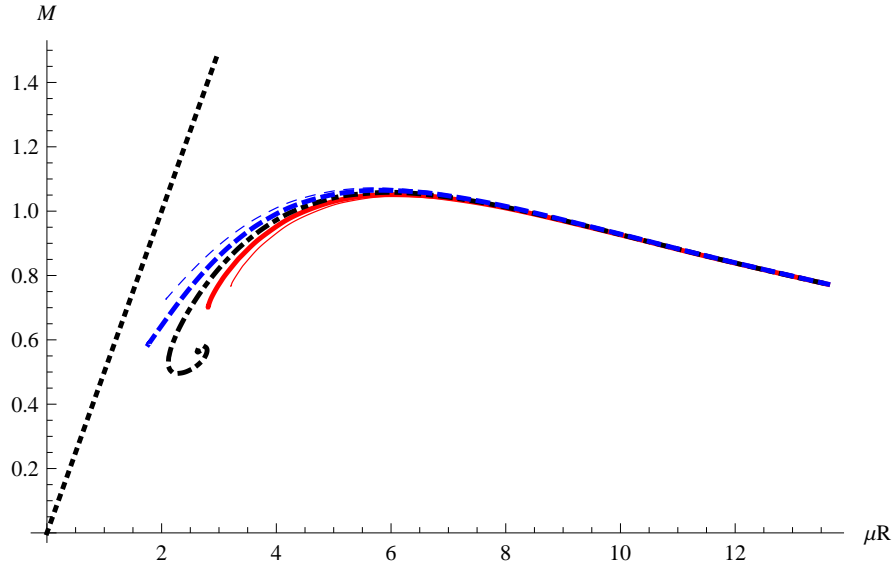


FIG. 7. M is shown as a function of $\mu\mathcal{R}$. The solid red, thick red, thick black dotted-dashed, thick blue dashed, and blue dashed curves correspond to $\beta = 0.2, 0.1, 0, -0.1$, and -0.2 , respectively, and the black dotted line represents $\mathcal{R} = 2m_\infty$. Here, M is shown in M_p^2/μ .

In Figs. 8-10, for $\beta = 0, 0.2$, and -0.2 , M and μQ are shown as functions of $\mu\mathcal{R}$, respectively. For all $\beta = 0, 0.2$, and -0.2 , for $\mu\mathcal{R} \gtrsim 3.5$, Eq. (18) is satisfied, while for $\mu\mathcal{R} \lesssim 3.5$, it is not satisfied.

D. Compactness

In Fig. 11, for $\beta = 0.2, 0$, and -0.2 , \mathcal{C} as defined in Eq. (20) is shown as the function of $\mu\mathcal{R}$. For $\mu\mathcal{R} \gtrsim 6.0$, \mathcal{C} becomes smaller and no clear β dependence is observed, while for $\mu\mathcal{R} \lesssim 6.0$, β dependence becomes more evident and a larger (smaller) value of \mathcal{C} is observed for $\beta < 0$ ($\beta > 0$). For $\beta = 0$, \mathcal{C} is a multivalued function of \mathcal{R} , while for $\beta \neq 0$, it is a single-valued function of \mathcal{R} .

For $\beta = 0$, as f_0 increases, \mathcal{R} decreases, and \mathcal{C} increases and takes the maximal value 0.280 for $\mu\mathcal{R} \approx 2.50$. After reaching the maximal value, \mathcal{C} starts to decrease, while $\mu\mathcal{R}$ still decreases and reaches the minimal value 2.12. As f_0 further increases, \mathcal{C} eventually converges to 0.213.

For $\beta = 0.2$, as f_0 increases while $\mu\mathcal{R}$ decreases, \mathcal{C} increases, takes the maximal value 0.243 for $\mu\mathcal{R} \approx 3.44$, and then decreases until $\mu\mathcal{R}$ reaches the minimal value 3.21.

For $\beta = -0.2$, as f_0 increases while $\mu\mathcal{R}$ decreases \mathcal{C} monotonically increases and takes the maximal value 0.350 when $\mu\mathcal{R}$ reaches the minimal value 2.08 due to the technical problem discussed in Sec. IV A. There may be PS solutions for $\mu\mathcal{R} \lesssim 2.08$, for which \mathcal{C} may be larger values than 0.350. However, the condition (18) is not satisfied for such solutions.

E. Speculation about stability

Although in the given subclass of the generalized complex Proca theory the explicit analysis of stability will be quite involved, in this subsection we will give the speculation about stability in terms of the insensitivity of the critical central amplitude of the

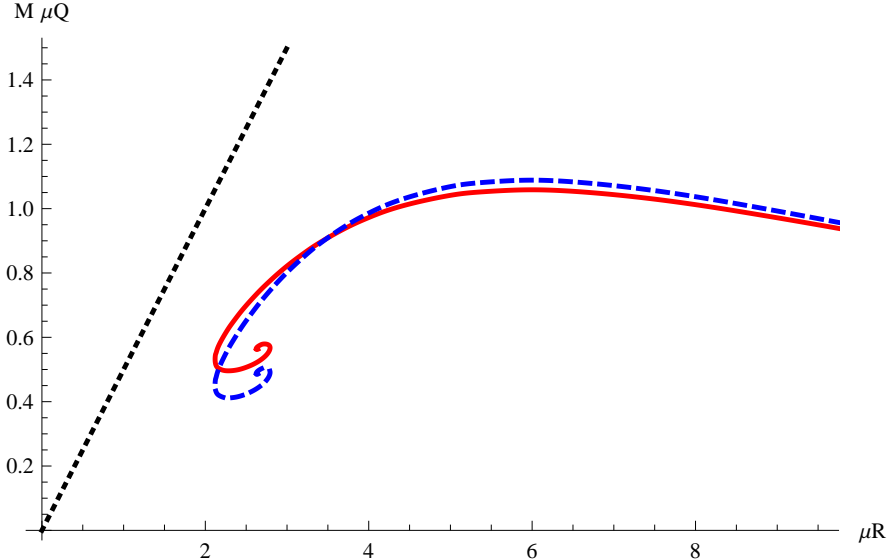


FIG. 8. M and μQ are shown as functions of μR , for $\beta = 0$. The solid red and blue dashed curves correspond to M and μQ , respectively, and the black dotted line represents $\mathcal{R} = 2m_\infty$. Here, M and μQ are shown in M_p^2/μ .

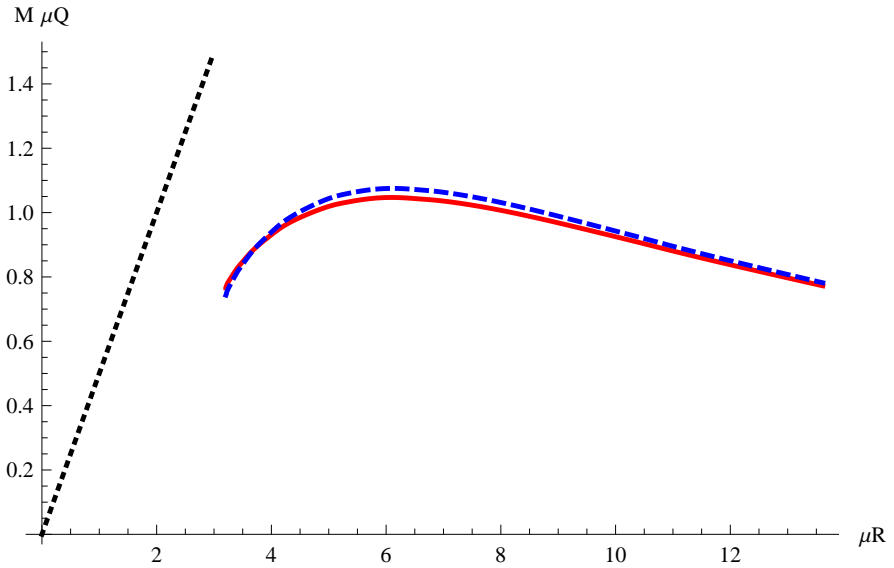


FIG. 9. M and μQ are shown as functions of μR , for $\beta = 0.2$. The solid red and blue dashed curves correspond to M and μQ , respectively, and the black dotted line represents $\mathcal{R} = 2m_\infty$. Here, M and μQ are shown in M_p^2/μ .

vector field $f_{0,c}$, for which PSs take the maximal values of the ADM mass M and the Noether charge Q , to the choice of the nonminimal coupling parameter β .

We have confirmed that the value of the critical central amplitude, which in our analysis is found to be $f_{0,c} \approx 0.0399M_p$, is insensitive to the choice of β , although the absolute maximal values of M and μQ both depend on β . As we have mentioned in Sec. I, in the case of $\beta = 0$ the PS solution with the maximal values of M and μQ corresponds to the critical solution which divides stable and unstable PS solutions [33], as in the case of BSs in the scalar-tensor theory [27, 28]. Thus, the insensitivity of the value of $f_{0,c}$ to the choice of β indicates that even in the presence of nonminimal coupling $\beta \neq 0$ the PS solution with the maximal values of M and μQ obtained for $f_{0,c} \approx 0.0399M_p$ would also correspond to the critical PS solution which divides stable and unstable PS ones, and PS solutions for $f_0 < f_{0,c} \approx 0.0399M_p$ would be stable, irrespective of the choice of β . The explicit confirmation of this speculation is definitely important, but will be left for future studies.

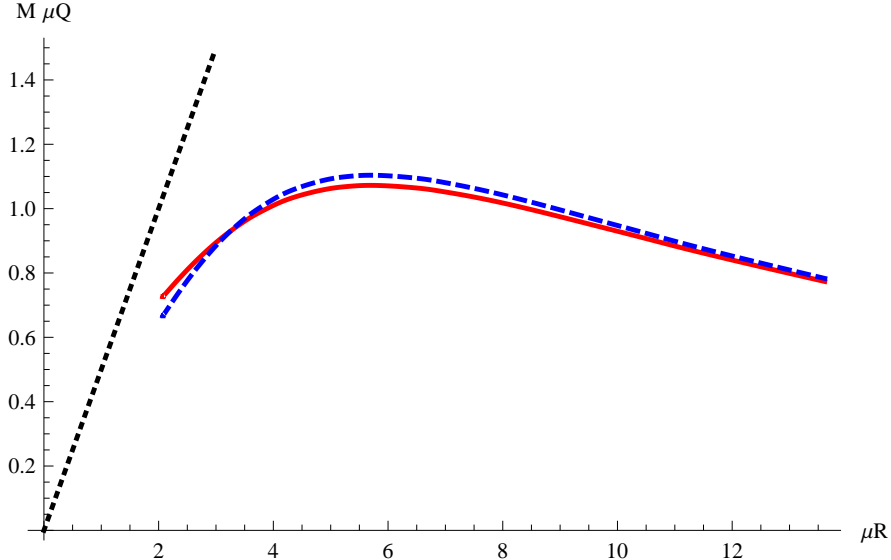


FIG. 10. M and μQ are shown as functions of μR , for $\beta = -0.2$. The solid red and blue dashed curves correspond to M and μQ , respectively, and the black dotted line represents $\mathcal{R} = 2m_\infty$. Here, M and μQ are shown in M_p^2/μ .

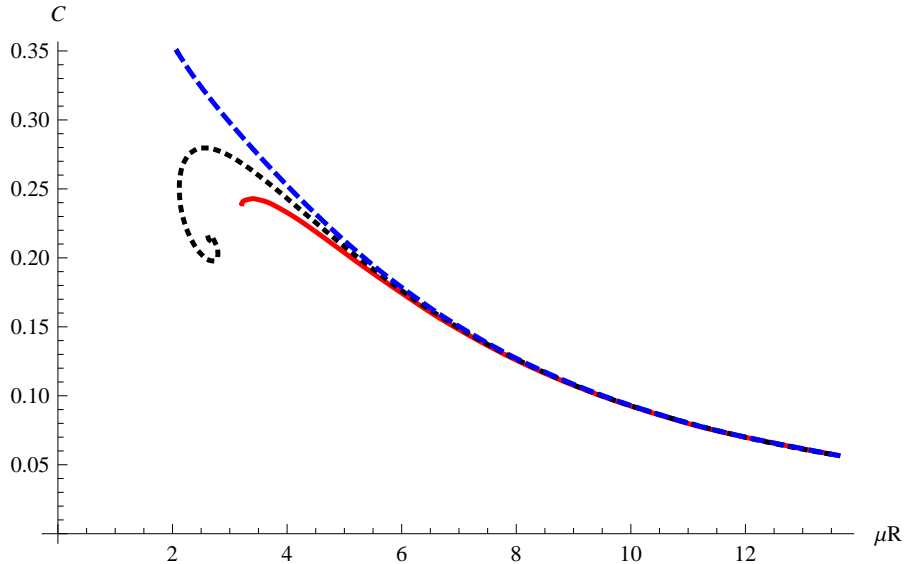


FIG. 11. C is shown as the function of μR . The solid red, black dotted, and blue dashed curves correspond to $\beta = 0.2, 0$, and -0.2 , respectively.

V. CONCLUSIONS

In this paper, we have investigated boson star type solutions in the generalized complex Proca theory with mass and nonminimal coupling to the Einstein tensor, namely Proca star solutions. We have numerically constructed PS solutions for nonzero values of the nonminimal coupling parameter, and found that the inclusion of it changes properties of PSs.

For positive nonminimal coupling parameters, PS solutions did not exist for central amplitudes above some certain value, as the evolution equations to determine the structure of PSs became singular at very small radii. For negative nonminimal coupling parameters, although there was no such singular behavior, sufficiently enhanced numerical resolutions were requested for larger amplitudes. Thus, for larger absolute values of the nonminimal coupling parameter, spiraling features observed for the vanishing nonminimal coupling eventually disappeared. Moreover, for negative (positive) nonminimal coupling parameters, for the same

frequency PSs had larger (smaller) ADM mass and Noether charge than those for the vanishing nonminimal coupling parameter. Irrespective of the sign of the nonzero nonminimal coupling parameter, PSs with the maximal values of the ADM mass and the Noether charge were always gravitationally bound.

Such behaviors of PSs were similar to those observed for BSs in the EGB theory [30, 31], EdGB theory [32], and complex scalar-tensor theory with nonminimal derivative coupling to the Einstein tensor [29]. Thus, they would be generic for gravitational theories including healthy higher-derivative terms. Similarities between the scalar-tensor and generalized Proca theories with nonminimal coupling to the Einstein tensor were pointed out in the context of BH physics in Refs. [14, 15, 17, 18].

Finally, we have given the speculation on stability of PSs in the given subclass of the generalized complex theory. We have confirmed that the critical central amplitude of the vector field which provides the PS solutions with the maximal values of the ADM mass and the Noether charge is insensitive to the choice of the nonminimal coupling parameter. Since, in the case without nonminimal coupling, the PS solution with the maximal values of ADM mass and Noether charge corresponds to the critical PS solution dividing stable and unstable PS solutions [33], combined with the confirmed insensitivity to the choice of the nonminimal coupling parameter, we have speculated that even in the presence of nonzero nonminimal coupling PS solutions with the maximal values of ADM mass and Noether charge correspond to the critical PS solutions dividing stable and unstable PS ones. The explicit confirmation of this speculation will be left for the future studies.

PS solutions obtained in this paper were mini-BS type. A definitively interesting question is whether more massive PS solutions can be constructed in the presence of self-couplings and other nonminiaml couplings to curvatures. We will leave these issues for our future studies.

ACKNOWLEDGEMENTS

This work was supported by FCT-Portugal through Grant No. SFRH/BPD/88299/2012. We thank Vishal Baibhav for comments.

Appendix A: Components of EOMs

The (\hat{t}, \hat{t}) , (r, r) , and angular components of the gravitational EOM (10) are given by

$$\mathcal{E}^{\hat{t}}_{\hat{t}} = -\frac{1}{2r^4\kappa^2(r-2m(r))\sigma(r)^2}U^{\hat{t}}_{\hat{t}}(r), \quad (\text{A1a})$$

$$\mathcal{E}^r_r = \frac{1}{2r^3\kappa^2(r-2m(r))\sigma(r)^3}U^r_r(r), \quad (\text{A1b})$$

$$\mathcal{E}^i_i = \frac{1}{r^4\kappa^2(r-2m(r))^2\sigma(r)^4}U^i_i(r), \quad (\text{A1c})$$

where

$$U^{\hat{t}}(r) := r^3 \kappa^2 a_0(r)^2 (\mu^2 r^2 + 2\beta m'(r)) + (r - 2m(r)) \left[r^4 \kappa^2 a_0'(r)^2 - 2r \kappa^2 a_1(r) (r^3 \hat{\omega} a_0'(r) - 2\beta (r - 2m(r))^2 \sigma(r)^2 a_1'(r)) - 4r^2 \sigma(r)^2 m'(r) + \kappa^2 a_1(r)^2 \left\{ r^4 \hat{\omega}^2 + (r - 2m(r)) \sigma(r)^2 (\mu^2 r^3 + 2r\beta + 4\beta m(r) - 6r\beta m'(r)) \right\} \right], \quad (\text{A2a})$$

$$U^r(r) = -4r^2 \beta \kappa^2 a_0(r) (r - 2m(r)) \sigma(r) a_0'(r) + r \kappa^2 a_0(r)^2 \left(\sigma(r) (\mu^2 r^3 + 4\beta m(r) - 2r\beta m'(r)) + 2r\beta (r - 2m(r)) \sigma'(r) \right) - (r - 2m(r)) \sigma(r) \left[-2r^3 \kappa^2 \hat{\omega} a_1(r) a_0'(r) + \kappa^2 a_1(r)^2 \left\{ r^3 \hat{\omega}^2 - (r - 2m(r)) \sigma(r)^2 (\mu^2 r^2 - 2\beta + 6\beta m'(r)) + 6\beta (r - 2m(r))^2 \sigma(r) \sigma'(r) \right\} + r \left\{ r^2 \kappa^2 a_0'(r)^2 - 4\sigma(r) (\sigma(r) m'(r) - (r - 2m(r)) \sigma'(r)) \right\} \right], \quad (\text{A2b})$$

$$U^i(r) = -2r^3 \beta \kappa^2 a_0(r) (r - 2m(r)) \sigma(r) \times \left[-2r(r - 2m(r)) a_0'(r) \sigma'(r) + \sigma(r) \left(a_0'(r) (r - 3m(r) + rm'(r)) + r(r - 2m(r)) a_0''(r) \right) \right] + r^2 \kappa^2 a_0(r)^2 \left[-2r^2 \beta (r - 2m(r))^2 \sigma'(r)^2 + \sigma(r)^2 \left\{ 2\beta m(r)^2 - 2rm(r) (\mu^2 r^2 + \beta - r\beta m''(r)) + r^2 (\mu^2 r^2 + 2\beta m'(r) - 2\beta m'(r)^2 - r\beta m''(r)) \right\} + r\beta (r - 2m(r)) \sigma(r) \left((r - 3m(r) + rm'(r)) \sigma'(r) + r(r - 2m(r)) \sigma''(r) \right) + (r - 2m(r))^2 \sigma(r)^2 \left[-2r \kappa^2 a_1(r) \left(r^3 \hat{\omega} a_0'(r) + \beta (r - 2m(r)) \sigma(r) a_1'(r) (-\sigma(r) (m(r) + r(-1 + m'(r))) + r(r - 2m(r)) \sigma'(r)) \right) + \kappa^2 a_1(r)^2 \left\{ r^4 \hat{\omega}^2 + \sigma(r)^2 \left(2\beta m(r)^2 + 2rm(r) (\mu^2 r^2 - \beta - r\beta m''(r)) + r^2 (-\mu^2 r^2 + 2\beta m'(r) - 2\beta m'(r)^2 + r\beta m''(r)) - r\beta (r - 2m(r)) \sigma(r) ((r + 3m(r) - 5rm'(r)) \sigma'(r) + r(r - 2m(r)) \sigma''(r)) \right\} + r^2 \left\{ r^2 (1 - 2\beta) \kappa^2 a_0'(r)^2 + 2\sigma(r) \left[-r(r + m(r) - 3rm'(r)) \sigma'(r) + r(\sigma(r) m''(r) - (r - 2m(r)) \sigma''(r)) \right] \right\} \right] \right], \quad (\text{A2c})$$

respectively.

The \hat{t} and r components of the vector field EOM (11) are given by

$$\mathcal{F}_{\hat{t}} = \frac{e^{-i\hat{\omega}\hat{t}}}{r^2 \sigma(r)} V_{\hat{t}}(r), \quad (\text{A3a})$$

$$\mathcal{F}_r = -\frac{ie^{-i\hat{\omega}\hat{t}}}{r^2 (r - 2m(r)) \sigma(r)^2} V_r(r), \quad (\text{A3b})$$

where

$$V_{\hat{t}}(r) := -a_0(r) \sigma(r) (\mu^2 r^2 + 2\beta m'(r)) + (r - 2m(r)) (-ra_0'(r) \sigma'(r) + a_1(r) (-2\hat{\omega} \sigma(r) + r\hat{\omega} \sigma'(r)) + \sigma(r) (2a_0'(r) - r\hat{\omega} a_1'(r) + ra_0''(r))), \quad (\text{A4a})$$

$$V_r(r) := r^3 \hat{\omega} a_0'(r) - a_1(r) \left(r^3 \hat{\omega}^2 - (r - 2m(r)) \sigma(r)^2 (\mu^2 r^2 + 2\beta m'(r)) + 2\beta (r - 2m(r))^2 \sigma(r) \sigma'(r) \right), \quad (\text{A4b})$$

respectively.

The constraint relation (6) is given by

$$\mathcal{G} = \frac{ie^{-i\hat{\omega}\hat{t}}}{r^4 (r - 2m(r)) \sigma(r)^2} W(r), \quad (\text{A5})$$

where

$$\begin{aligned}
W(r) := & r^3 \hat{\omega} a_0(r) (\mu^2 r^2 + 2\beta m'(r)) \\
& + (r - 2m(r)) \sigma(r) \left[r(r - 2m(r)) a'_1(r) (\sigma(r) (\mu^2 r^2 + 2\beta m'(r)) - 2\beta(r - 2m(r)) \sigma'(r)) \right. \\
& + a_1(r) \left\{ -2\sigma(r) \left(r(\mu^2 r^2 m'(r) + 2\beta m'(r)^2 - r(\mu^2 r + \beta m''(r))) + m(r) (-2\beta m'(r) + r(\mu^2 r + 2\beta m''(r))) \right) \right. \\
& \left. \left. + (r - 2m(r)) \left((\mu^2 r^2 - 2r\beta - 4\beta m(r) + 10r\beta m'(r)) \sigma'(r) - 2r\beta(r - 2m(r)) \sigma''(r) \right) \right\} \right]. \tag{A6}
\end{aligned}$$

These equations are constrained by Eq. (12).

Appendix B: Evolution equations

Combining $\mathcal{E}^r_r = 0$, $\mathcal{E}^{\hat{t}}_{\hat{t}} = 0$, and $\mathcal{F}_{\hat{t}} = 0$ in Eqs. (A1) and (A3), we obtain the evolution equations for $m(r)$, $\sigma(r)$, and $a'_0(r)$ as

$$\begin{aligned}
m'(r) = & -\frac{\kappa^2}{2r[r^2\beta\kappa^2a_0(r)^2 - (2r + 3\beta\kappa^2a_1(r)^2(r - 2m(r)))(r - 2m(r))\sigma(r)^2]} \\
& \times \left\{ \mu^2 r^5 a_0(r)^2 + (r - 2m(r)) \left[a_1(r)^2 (r^4 \hat{\omega}^2 + (r - 2m(r))(\mu^2 r^3 + 2r\beta + 4\beta m(r))\sigma(r)^2) \right. \right. \\
& \left. \left. + r^4 a'_0(r)^2 - 2ra_1(r)(r^3 \hat{\omega} a'_0(r) - 2\beta(r - 2m(r))^2 \sigma(r)^2 a'_1(r)) \right] \right\}, \tag{B1a}
\end{aligned}$$

$$\begin{aligned}
\sigma'(r) = & -\frac{\kappa^2 \sigma(r)}{r(r - 2m(r)) [r^2\beta\kappa^2a_0(r)^2 - (2r + 3\beta\kappa^2a_1(r)^2(r - 2m(r)))(r - 2m(r))\sigma(r)^2]} \\
& \times \left\{ a_0(r)^2 (\mu^2 r^5 + 2r^2 \beta m(r)) - 2r^3 \beta a_0(r)(r - 2m(r)) a'_0(r) \right. \\
& \left. + a_1(r)(r - 2m(r))^2 \sigma(r)^2 [a_1(r)(\mu^2 r^3 + 2\beta m(r)) + 2r\beta(r - 2m(r)) a'_1(r)] \right\}, \tag{B1b}
\end{aligned}$$

$$\begin{aligned}
a''_0(r) = & \frac{1}{r(r - 2m(r))} \times \left\{ \mu^2 r^2 a_0(r) + 2r\hat{\omega} a_1(r) - 4\hat{\omega} a_1(r)m(r) - 2ra'_0(r) + 4m(r)a'_0(r) \right. \\
& + \frac{r\kappa^2(\hat{\omega} a_1(r) - a'_0(r))}{2r^2\beta\kappa^2a_0(r)^2 - 2(2r + 3\beta\kappa^2a_1(r)^2(r - 2m(r)))(r - 2m(r))\sigma(r)^2} \\
& \times \left[a_0(r)^2 (\mu^2 r^4 + 4r\beta m(r)) - 4r^2 \beta a_0(r)(r - 2m(r)) a'_0(r) \right. \\
& - (r - 2m(r)) \left(a_1(r)^2 (r^3 \hat{\omega}^2 - (\mu^2 r^2 - 2\beta)(r - 2m(r))\sigma(r)^2) - 2r^3 \hat{\omega} a_1(r) a'_0(r) + r^3 a'_0(r)^2 \right) \\
& + r^2 \hat{\omega} a'_1(r) - 2r\hat{\omega} m(r) a'_1(r) \\
& + \frac{\kappa^2(-2\beta a_0(r) + r\hat{\omega} a_1(r) - ra'_0(r))}{2r(r^2\beta\kappa^2a_0(r)^2 - (2r + 3\beta\kappa^2a_1(r)^2(r - 2m(r)))(r - 2m(r))\sigma(r)^2)} \\
& \times \left[\mu^2 r^5 a_0(r)^2 + (r - 2m(r)) \left(a_1(r)^2 (r^4 \hat{\omega}^2 + (r - 2m(r))(\mu^2 r^3 + 2r\beta + 4\beta m(r))\sigma(r)^2) \right. \right. \\
& \left. \left. + r^4 a'_0(r)^2 - 2ra_1(r)(r^3 \hat{\omega} a'_0(r) - 2\beta(r - 2m(r))^2 \sigma(r)^2 a'_1(r)) \right) \right] \right\}. \tag{B1c}
\end{aligned}$$

Then, $\mathcal{E}^i_i = 0$ in Eq. (A1) and $\mathcal{G} = 0$ (A5) contain the combination

$$m''(r) - (r - 2m(r)) \frac{\sigma''(r)}{\sigma(r)}. \tag{B2}$$

By combining them, we obtain

$$a''_0(r) = \mathcal{C} [a_0(r), a_1(r), a'_0(r), a'_1(r), m(r), \sigma(r), m'(r), \sigma'(r)], \tag{B3}$$

where \mathcal{C} is the nonlinear combination of the given variables, which is too involved to be shown explicitly. Then substituting Eqs. (B1) into Eq. (B3), we can replace $m'(r)$, $\sigma'(r)$, and $a''_0(r)$ in Eq. (B3) with the lower derivative terms, and obtain the equation

$$\tilde{\mathcal{C}}_0 [a_0(r), a_1(r), a'_0(r), m(r), \sigma(r)] + \tilde{\mathcal{C}}_1 [a_0(r), a_1(r), a'_0(r), m(r), \sigma(r)] a'_1(r) = 0, \tag{B4}$$

where \tilde{C}_i ($i = 0, 1$) are the nonlinear combinations of the given variables, which are too involved to be shown explicitly. Hence, we can solve Eq. (B4) in terms of $a'_1(r)$ as

$$a'_1(r) = -\frac{\tilde{C}_0 [a_0(r), a_1(r), a'_0(r), m(r), \sigma(r)]}{\tilde{C}_1 [a_0(r), a_1(r), a'_0(r), m(r), \sigma(r)]}. \quad (\text{B5})$$

BS solutions do not exist if $\tilde{C}_1 [a_0(r), a_1(r), a'_0(r), m(r), \sigma(r)]$ vanishes at some radius.

[1] Timothy Clifton, Pedro G. Ferreira, Antonio Padilla, and Constantinos Skordis, “Modified Gravity and Cosmology,” *Phys.Rept.* **513**, 1–189 (2012), [arXiv:1106.2476 \[astro-ph.CO\]](#).

[2] Emanuele Berti *et al.*, “Testing General Relativity with Present and Future Astrophysical Observations,” *Class. Quant. Grav.* **32**, 243001 (2015), [arXiv:1501.07274 \[gr-qc\]](#).

[3] Gregory Walter Horndeski, “Second-order scalar-tensor field equations in a four-dimensional space,” *Int.J.Theor.Phys.* **10**, 363–384 (1974).

[4] C. Deffayet, S. Deser, and G. Esposito-Farèse, “Generalized Galileons: All scalar models whose curved background extensions maintain second-order field equations and stress-tensors,” *Phys. Rev.* **D80**, 064015 (2009), [arXiv:0906.1967 \[gr-qc\]](#).

[5] C. Deffayet, Xian Gao, D.A. Steer, and G. Zahariade, “From k-essence to generalised Galileons,” *Phys.Rev.* **D84**, 064039 (2011), [arXiv:1103.3260 \[hep-th\]](#).

[6] Tsutomu Kobayashi, Masahide Yamaguchi, and Jun’ichi Yokoyama, “Generalized G-inflation: Inflation with the most general second-order field equations,” *Prog. Theor. Phys.* **126**, 511–529 (2011), [arXiv:1105.5723 \[hep-th\]](#).

[7] Gianmassimo Tasinato, “Cosmic Acceleration from Abelian Symmetry Breaking,” *JHEP* **04**, 067 (2014), [arXiv:1402.6450 \[hep-th\]](#).

[8] Lavinia Heisenberg, “Generalization of the Proca Action,” *JCAP* **1405**, 015 (2014), [arXiv:1402.7026 \[hep-th\]](#).

[9] Erwan Ally, Patrick Peter, and Yeinzon Rodriguez, “Generalized Proca action for an Abelian vector field,” *JCAP* **1602**, 004 (2016), [arXiv:1511.03101 \[hep-th\]](#).

[10] Jose Beltran Jimenez and Lavinia Heisenberg, “Derivative self-interactions for a massive vector field,” *Phys. Lett.* **B757**, 405–411 (2016), [arXiv:1602.03410 \[hep-th\]](#).

[11] Antonio De Felice, Lavinia Heisenberg, Ryotaro Kase, Shinji Tsujikawa, Ying-li Zhang, and Gong-Bo Zhao, “Screening fifth forces in generalized Proca theories,” *Phys. Rev.* **D93**, 104016 (2016), [arXiv:1602.00371 \[gr-qc\]](#).

[12] Antonio De Felice, Lavinia Heisenberg, Ryotaro Kase, Shinji Mukohyama, Shinji Tsujikawa, and Ying-li Zhang, “Cosmology in generalized Proca theories,” *JCAP* **1606**, 048 (2016), [arXiv:1603.05806 \[gr-qc\]](#).

[13] Antonio De Felice, Lavinia Heisenberg, Ryotaro Kase, Shinji Mukohyama, Shinji Tsujikawa, and Ying-li Zhang, “Effective gravitational couplings for cosmological perturbations in generalized Proca theories,” *Phys. Rev.* **D94**, 044024 (2016), [arXiv:1605.05066 \[gr-qc\]](#).

[14] Javier Chagoya, Gustavo Niz, and Gianmassimo Tasinato, “Black Holes and Abelian Symmetry Breaking,” *Class. Quant. Grav.* **33**, 175007 (2016), [arXiv:1602.08697 \[hep-th\]](#).

[15] Masato Minamitsuji, “Solutions in the generalized Proca theory with the nonminimal coupling to the Einstein tensor,” *Phys. Rev.* **D94**, 084039 (2016), [arXiv:1607.06278 \[gr-qc\]](#).

[16] Wei-Jian Geng and H. Lu, “Einstein-Vector Gravity, Emerging Gauge Symmetry and de Sitter Bounce,” *Phys. Rev.* **D93**, 044035 (2016), [arXiv:1511.03681 \[hep-th\]](#).

[17] Javier Chagoya, Gustavo Niz, and Gianmassimo Tasinato, “Black Holes and Neutron Stars in Vector Galileons,” (2017), [arXiv:1703.09555 \[gr-qc\]](#).

[18] Eugeny Babichev, Christos Charmousis, and Mokhtar Hassaine, “Black holes and solitons in an extended Proca theory,” *JHEP* **05**, 114 (2017), [arXiv:1703.07676 \[gr-qc\]](#).

[19] Lavinia Heisenberg, Ryotaro Kase, Masato Minamitsuji, and Shinji Tsujikawa, “Hairy black-hole solutions in generalized Proca theories,” (2017), [arXiv:1705.09662 \[gr-qc\]](#).

[20] David J. Kaup, “Klein-Gordon Geon,” *Phys. Rev.* **172**, 1331–1342 (1968).

[21] Remo Ruffini and Silvano Bonazzola, “Systems of selfgravitating particles in general relativity and the concept of an equation of state,” *Phys. Rev.* **187**, 1767–1783 (1969).

[22] R. Friedberg, T. D. Lee, and Y. Pang, “MINI - SOLITON STARS,” *Phys. Rev.* **D35**, 3640 (1987), [,55(1986)].

[23] Philippe Jetzer, “Boson stars,” *Phys. Rept.* **220**, 163–227 (1992).

[24] F.E. Schunck and E.W. Mielke, “General relativistic boson stars,” *Class.Quant.Grav.* **20**, R301–R356 (2003), [arXiv:0801.0307 \[astro-ph\]](#).

[25] Marcelo Gleiser, “Stability of Boson Stars,” *Phys. Rev.* **D38**, 2376 (1988), [Erratum: *Phys. Rev.* D39,no.4,1257(1989)].

[26] T. D. Lee and Yang Pang, “Stability of Mini - Boson Stars,” *Nucl. Phys.* **B315**, 477 (1989), [,129(1988)].

[27] Marcelo Gleiser and Richard Watkins, “Gravitational Stability of Scalar Matter,” *Nucl. Phys.* **B319**, 733–746 (1989).

[28] Scott H. Hawley and Matthew W. Choptuik, “Boson stars driven to the brink of black hole formation,” *Phys. Rev.* **D62**, 104024 (2000), [arXiv:gr-qc/0007039 \[gr-qc\]](#).

[29] Yves Brihaye, Adolfo Cisterna, and Cristian Erices, “Boson stars in biscalar extensions of Horndeski gravity,” *Phys. Rev.* **D93**, 124057 (2016), [arXiv:1604.02121 \[hep-th\]](#).

[30] Betti Hartmann, Jurgen Riedel, and Raluca Suci, “Gauss-Bonnet boson stars,” *Phys. Lett.* **B726**, 906–912 (2013), [arXiv:1308.3391 \[gr-qc\]](#).

- [31] Yves Brihaye and Jurgen Riedel, “Rotating boson stars in five-dimensional Einstein-Gauss-Bonnet gravity,” *Phys. Rev.* **D89**, 104060 (2014), arXiv:1310.7223 [gr-qc].
- [32] Vishal Baibhav and Debaprasad Maity, “Boson Stars in Higher Derivative Gravity,” *Phys. Rev.* **D95**, 024027 (2017), arXiv:1609.07225 [gr-qc].
- [33] Richard Brito, Vitor Cardoso, Carlos A. R. Herdeiro, and Eugen Radu, “Proca stars: Gravitating Bose-Einstein condensates of massive spin 1 particles,” *Phys. Lett.* **B752**, 291–295 (2016), arXiv:1508.05395 [gr-qc].
- [34] Ignacio Salazar Landea and Federico Garcia, “Charged Proca Stars,” *Phys. Rev.* **D94**, 104006 (2016), arXiv:1608.00011 [hep-th].
- [35] Y. Brihaye, Th. Delplace, and Y. Verbin, “Proca Q Balls and their Coupling to Gravity,” (2017), arXiv:1704.01648 [gr-qc].
- [36] Richard P. Woodard, “Ostrogradsky’s theorem on Hamiltonian instability,” *Scholarpedia* **10**, 32243 (2015), arXiv:1506.02210 [hep-th].
- [37] G. H. Derrick, “Comments on nonlinear wave equations as models for elementary particles,” *J. Math. Phys.* **5**, 1252–1254 (1964).